processes

MDPI

Article

Numerical Prediction of Refrigerant Oil Two-Phase Flow from Scroll Compressor Discharge to the Suction Side via Back Pressure Chamber

Vladimir D. Stevanovic [1,*], Milan M. Petrovic [1], Stojan Cucuz [2], Sanja Milivojevic [1] and Milica Ilic [3]

[1] Faculty of Mechanical Engineering, University of Belgrade, Kraljice Marije 16, 11120 Belgrade, Serbia; mlpetrovic@mas.bg.ac.rs (M.M.P.); smilivojevic@mas.bg.ac.rs (S.M.)
[2] Pierburg GmbH, Alfred-Pierburg-Straße 1, 41460 Neuss, Germany; stojan.cucuz@de.rheinmetall.com
[3] Innovation Center, Faculty of Mechanical Engineering, University of Belgrade, Kraljice Marije 16, 11120 Belgrade, Serbia; milic@mas.bg.ac.rs
* Correspondence: vstevanovic@mas.bg.ac.rs; Tel.: +381-11-3370-561

Abstract: Oil lubricates the contact between the orbiting and stationary scroll in the refrigerant scroll compressor, while the sealing between the scrolls is achieved through the refrigerant vapour pressure in the sealed back pressure chamber. The back pressure should be adjusted using the refrigerant oil two-phase flow from the oil separator at the compressor discharge to the back pressure chamber and the refrigerant oil flow from the back pressure chamber to the compressor suction side. Both of the flows are conducted through connecting tubes with corresponding high-pressure and low-pressure nozzles with small diameters. Models for predicting the refrigerant oil critical and subcritical flows through the nozzles were developed and applied in enable the prediction of the back pressure. The models are original, because the slip between the oil and the refrigerant as well as the refrigerant solubility in the oil are taken into account. The critical flow model is validated against the experimental data that are available in the literature. The back pressure is predicted by equating the mass flow rates of refrigerant and oil two-phase mixtures through the high- and low-pressure nozzles. The results show that the critical flow takes place through the high-pressure nozzle, while the subcritical flow through the low-pressure nozzle can also exist in cases with a small pressure difference between the back pressure chamber and the compressor suction side. The refrigerant solubility in the oil has a small influence on the critical and subcritical refrigerant oil mixture mass flow rates, while the influence on the back pressure is more pronounced.

Keywords: refrigerant; oil; two-phase critical flow; scroll compressor; back pressure chamber

Citation: Stevanovic, V.D.; Petrovic, M.M.; Cucuz, S.; Milivojevic, S.; Ilic, M. Numerical Prediction of Refrigerant Oil Two-Phase Flow from Scroll Compressor Discharge to the Suction Side via Back Pressure Chamber. *Processes* **2024**, *12*, 6. https://doi.org/10.3390/pr12010006

Academic Editor: Iztok Golobič

Received: 20 November 2023
Revised: 12 December 2023
Accepted: 15 December 2023
Published: 19 December 2023

1. Introduction

The compression of refrigerant vapour in scroll compressors is achieved through orbiting the driven scroll within the stationary scroll. The scroll compressors can be realized as follows: (a) The low side configurations occur with the refrigerant's high pressure in the discharge chamber following that of the stationary scroll; meanwhile, the rest of the compressor shell on the inner side is exposed to the refrigerant's low suction pressure. (b) The high side configurations occur; here, the whole compressor shell on the inner side is exposed to the refrigerant's discharge pressure; meanwhile, the inlet low-pressure refrigerant is led directly into the suction chamber of the working scrolls. (c) A partition configuration occurs; this is a hybrid design of the discharge's high pressure and the suction's low-pressure chambers [1]. The important issue of the scroll compressor design and operation a result of the provision of adequate lubrication between the orbiting and the stationary scrolls; however, here, there is minimum leakage through the minimized clearance areas [2]. In the low side scroll compressor, the uniformity of the sealing between the tips of the scrolls and the plates of the opposite scrolls is achieved through the refrigerant's

vapour pressure in the sealed back pressure chamber [3]. The back pressure pushes the driven scroll towards the stationary scroll. The back pressure should be adjusted through the refrigerant vapour flow from the oil separator at the compressor discharge side towards the back pressure chamber through a microchannel with a high-pressure nozzle, as well as by the refrigerant flow from the back pressure chamber towards the compressor suction through a low-pressure nozzle. The oil separator at the discharge side is filled with the oil and the refrigerant. Therefore, the two-phase mixture of oil and refrigerant flows from the separator towards the back pressure chamber and from the back pressure chamber towards the compressor suction side (see Figure 1).

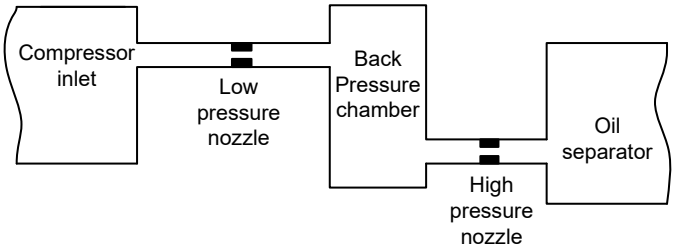

Figure 1. Scheme of the flow configuration.

Depending on the difference between the nozzle's upstream and downstream pressure, the two-phase flow through the nozzle can be either subcritical or critical (the latter is also known as choked flow). In case of a subcritical flow, the flow rate through the nozzle depends on the nozzle's dimensions, the upstream and downstream pressure differences, and the upstream two-phase flow parameters, such as the liquid and vapour phases' density and the two-phase mixture quality. In cases of critical flow, the flow rate also depends on the nozzle dimensions and the two-phase upstream mixture parameters, but is not affected by the downstream pressure: for the constant nozzle upstream parameters, the flow rate is constant, no matter what the value of the downstream pressure is. The sonic velocity at the location of the two-phase critical flow depends on the quality of the two-phase mixture, the two-phase flow pattern, the slip between the liquid and the vapour phase velocities, and the liquid-phase flashing. The non-linear dependence of the critical velocity on the aforementioned critical flow conditions might lead to a sonic velocity value that is lower than the sonic velocity in the vapour phase [4].

In order to provide efficient sealing between stationary and driven scrolls, the pressure in the back pressure chamber should be kept at a certain level under the variable load operation of the compressor. The scroll compressor load is varied by the variation of the orbiting speed of the driven scroll. The compressor load increase leads to the increase in two-phase mixture pressure, temperature, and quality in the oil separator at the compressor discharge. This means that, during the load change, there is a change in the two-phase mixture parameters in front of the nozzle between the oil separator and the back pressure chamber; this influences the two-phase mixture inflow that enters the back pressure chamber. These conditions pose a question: how can we construct nozzle and flow channels between the oil separator and the back pressure chamber, as well as between the back pressure chamber and the compressor suction side, that would provide adequate pressure levels in the back pressure chamber for ranges of compressor load variations? In order to provide the basis for the solution of this problem, it is necessary to predict the refrigerant oil two-phase flow from the oil separator to the back pressure chamber and from the back pressure chamber to the compressor suction side for a whole range of compressor operational load changes.

Previously conducted investigations of the two-component refrigerant and lubricating oil mixture flows were performed with the two-fluid mixtures of refrigerant liquid and vapour phase and oil liquid-phase. Experimental results on critical flows of refrigerant 134a and polyalkylene glycol–PAG oil through short tube orifices were presented in [5]. The oil mass fraction in the mixture with refrigerant was up to 5.1% and the refrigerant oil mixture in front of the orifice tube was subcooled and saturated, or two-phase mixture with

qualities as high as 0.08 are added. The thermal non-equilibrium with the liquid refrigerant superheating in the flow through the short tube orifice was observed. It was reported that the presence of oil may have delayed the onset of liquid refrigerant flashing. The presence of oil in the refrigerant led to the increase or decrease in the critical flow rate in comparison with the flow of pure refrigerant, depending on the upstream refrigerant subcooling or two-phase flow quality, while the maximum deviation was the decrease in the refrigerant oil mixture flow rate by 12.1% for a 5.1% oil concentration. The investigation of refrigerant R22's flow through a converging–diverging nozzle was reported in [6]. The refrigerant was slightly contaminated with lubricating oil, but its content was not determined. The refrigerant subcooling was 5–8 K at the nozzle inlet, while the liquid refrigerant flashing occurs in the nozzle due to the refrigerant acceleration and pressure drop. The critical flow was observed within the nozzle. Measured mass flow rates were compared with the values predicted with the homogeneous equilibrium model and the Henry–Fauske model of critical flow. The results of homogeneous equilibrium model deviate from the measured data in the range from −35% to 5%, while the Henry–Fauske model overpredicts the mass flow rate in the range from 15% to 35%. The experimental investigation of refrigerant R32 and oil flow through the electronic expansion valve was reported in [7]. It was shown that the oil has a slight influence on the refrigerant mass flow rate. An experimental correlation was developed for the prediction of R32 mass flow rate through the electronic expansion valve. The experimental and analytical investigation of two-phase water and steam flow rates in water-flooded twin-screw compressor was reported in [8]. In addition, methods were proposed for the prediction of discharge coefficients of orifices and nozzles. A model was presented in [9,10] for the prediction of pressure and mass of refrigerant and oil mixture in the back pressure chamber of the scroll compressor under transient conditions. Inlet and outlet flow rates of the refrigerant oil mixture at the back pressure chamber openings were modelled as subcritical. Unfortunately, no information on the flow channel dimensions and refrigerant and oil thermophysical characteristics are presented in [9,10]. As presented, the review of the open literature has shown that previous studies have mainly considered two-component two-phase flows of mixtures consisting of refrigerant liquid and gas-phases and liquid oil, which are characterized by thermal non-equilibrium and superheated liquid flashing. Therefore, there is a lack of information on refrigerant gas and liquid oil critical and subcritical flows; here, the important governing effect is the slip between the gas- and liquid-phase velocities. In addition, there is no information in the open-access literature on the prediction of the pressure in the back pressure chamber of the scroll compressors, which is subject to the chamber inlet and outlet flows under critical and subcritical conditions. Hence, the objectives of the research presented in this paper are detailed next.

This paper presents models for the calculation of critical and subcritical refrigerant gas and oil two-phase flows through nozzles, as well as predictions of the mass flow rates from the discharge to the suction side of the scroll compressor via the back pressure chamber and pressure values in the back pressure chamber, obtained for different discharge parameters. The non-homogeneous model of compressible refrigerant R744 (CO_2) and oil two-phase flow is applied. The influence of the slip between the liquid- and gas-phase velocities on the flow quality and vapour volume fraction is taken into account. The model is validated by the simulation of water and air critical flows, for which corresponding measured data are available in the literature. The pressure values in the back pressure chamber are derived from the predictions of CO_2 and oil flows through the compressors' high- and low-pressure nozzles. The influence of the oil mass fraction and the pressure level in the oil separator on the back pressure is shown. The refrigerant solubility in the oil is taken into account and its influence on the critical flow is evaluated. In the literature, there is a lack of information on the refrigerant and oil mixture critical flow. In addition, the influence of refrigerant-in-oil solubility on critical flow was not addressed. The developed models for the prediction of subcritical and critical flows of refrigerant and oil mixture are original, with a feature of taking into account the refrigerant solubility in oil. In general, the objective of the present research is to develop a reliable and robust engineering method

that is able to predict critical and subcritical mass flow rates of the refrigerant CO_2 gas and PAG oil mixture through nozzles. The final aim is the prediction of the pressure in the back pressure chamber of the scroll compressor through matching the calculated mass flow rates through the high-pressure and low-pressure nozzles of the compressor.

2. Modelling Approach

2.1. Geometry

Two-phase mixture flows of refrigerant R744 (CO_2) and polyalkylene glycol–PAG oil through a high-pressure and low-pressure nozzles are considered. The high-pressure nozzle has a diameter of 0.26 mm and it connects the oil separator and the back pressure chamber in the scroll compressor. The low-pressure nozzle has a diameter of 0.36 mm and it connects the back pressure chamber and the suction side of the compressor. The flow configuration is presented in Figure 1. Although the nozzles diameters are below 1 mm, these dimensions are still much greater than the microchannel dimensions that lead to the fluid rarefaction and fluid flow slip on the wall [11]. In addition, the pressure drop across the nozzles is rather high, being of several MPa or higher, which implies that the homogeneous spray of CO_2 gas with fine, small-diameter oil droplets flow through the nozzles.

2.2. Critical Flow

The complexity of critical two-phase flow prediction usually arises from the phenomena of velocity and thermal non-equilibrium [12]. The difference between gas- and liquid-phase velocities is known as the velocity non-equilibrium and it influences the gas-phase volume fraction in the two-phase flow, which strongly influences the two-phase critical mass flow rate. The thermal non-equilibrium arises in the critical flow with the liquid evaporation, when the limited evaporation rate cannot utilize the whole evaporation potential that arises during rapid pressure decrease and the liquid-phase becomes superheated. The thermal non-equilibrium also strongly influences the critical mass flow rate.

The present research is directed towards refrigerant gas and liquid oil two-phase flow. It is a two-component two-phase flow without phase transition; therefore, the thermal non-equilibrium plays no role, and it is not considered. Unlike thermal non-equilibrium, there is a difference between the liquid oil and refrigerant gas velocities; thus, the velocity non-equilibrium is taken into account and the flow is observed to be non-homogeneous.

Refrigerant R744 and oil critical flow in nozzles is modelled as two-component compressible two-phase flow. Solubility of CO_2 in oil is considered. The liquid phase consists of oil and dissolved CO_2, while the gas phase is CO_2 vapour. Isentropic flow is assumed from the upstream location, u-u, which is very close to the nozzle and the nozzle location, c-c, where the critical flow takes place, as presented in Figure 2.

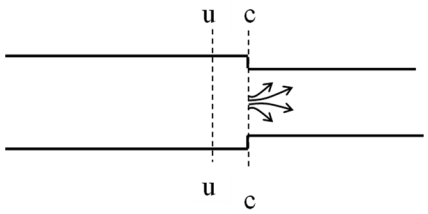

Figure 2. Locations of the critical flow (c-c) and the infinitesimal upstream (u-u) flow cross-section.

The mass balance for the flow from the upstream cross-section u-u (hereafter denoted with u) to the location of critical flow c-c (hereafter denoted with c) is formulated as:

$$u_u A_u \rho_u = u_c A_c \rho_c, \quad (1)$$

where u is the velocity, A is the area of flow cross-section, and ρ is the density. The energy equation for isentropic flow between cross-sections u and c is given by:

$$h_u + \frac{u_u^2}{2} = h_c + \frac{u_c^2}{2}, \tag{2}$$

where h is the enthalpy of two-phase flow mixture. Further, the following relation holds for the isentropic flow of ideal gas:

$$\frac{p_u}{\rho_u^\kappa} = \frac{p_c}{\rho_c^\kappa}, \tag{3}$$

where p represents the pressure and κ is the isentropic expansion coefficient.

Using the above relations and applying the ideal gas equation of state $(p = \rho R_g T)$, the enthalpy change can be formulated as:

$$h_c - h_u = c_p(T_c - T_u) = \frac{c_p}{R_g}\frac{p_u}{\rho_u}\left[\left(\frac{\rho_c}{\rho_u}\right)^{\kappa-1} - 1\right] = \frac{\kappa}{\kappa-1}\frac{p_u}{\rho_u}\left[\left(\frac{\rho_c}{\rho_u}\right)^{\kappa-1} - 1\right], \tag{4}$$

where T stands for the temperature, R_g is the gas constant, and c_p denotes the specific heat. At the location of critical isentropic flow, the two-phase mixture velocity equals the sonic velocity c:

$$u_c = c = \left(\frac{\partial p}{\partial \rho}\right)_s^{1/2} = \sqrt{\kappa p_c/\rho_c}. \tag{5}$$

Combining Equations (2) and (4) and using Equations (1), (3), and (5), the following relation can be derived for the ratio of two-phase mixture densities in cross-sections u and c:

$$\frac{\rho_c}{\rho_u} = \left(\frac{1 + \frac{\kappa-1}{2}\left(\frac{A_c}{A_u}\right)^2\left(\frac{\rho_c}{\rho_u}\right)^{\kappa+1}}{\frac{\kappa+1}{2}}\right)^{\frac{1}{\kappa-1}}. \tag{6}$$

The density ratio ρ_c/ρ_u is determined iteratively from Equation (6) for prescribed upstream conditions. The critical pressure p_c is calculated using Equation (3) and the critical velocity u_c is calculated from Equation (1). The isentropic expansion coefficient κ in the above equations is calculated from Equation (5):

$$\kappa = \frac{c^2}{p_c/\rho_c}. \tag{7}$$

The sonic velocity c in Equation (7) is calculated for the cross-section with the critical flow. For clarity, the subscript c denoting critical conditions is omitted in Equations (8)–(15). The evaluation of sonic velocity is performed applying the so-called "frozen two-phase sonic velocity" model [13] as follows:

$$c = \left[\frac{\alpha\rho}{\rho_2 c_2} + \frac{(1-\alpha)\rho}{\rho_1 c_1}\right]^{-1/2}. \tag{8}$$

In Equation (8) indices 1 and 2 denote the liquid and gas phases, respectively, while α is the CO_2 gas-phase volume fraction in the two-phase mixture; it is calculated as:

$$\alpha = \frac{1}{1 + \frac{1-\chi}{\chi} S \frac{\rho_2}{\rho_1}}. \tag{9}$$

The flow quality χ is evaluated as the ratio of gas-phase mass flow rate to the total mass flow rate of two-phase mixture:

$$\chi = \frac{\dot{m}_2}{\dot{m}_1 + \dot{m}_2}. \tag{10}$$

The velocity slip in Equation (9) is calculated with the following parametric function which combines the Chisholm correlation [14] for the lower quality values and the Zivi correlation [14] for the maximum value of the gas- and liquid-phase velocity slips:

$$S = \begin{cases} S_{Chislom},\ S_{Chislom} < S_{Zivi} \\ S_{Zivi},\ S_{Chislom} > S_{Zivi} \end{cases}, \tag{11}$$

where:

$$S_{Chisholm} = \left[1 + \chi\left(\frac{\rho_1}{\rho_2} - 1\right)\right]^{0.5}, \tag{12}$$

and

$$S_{Zivi} = \left(\frac{\rho_1}{\rho_2}\right)^{1/3}. \tag{13}$$

The mixture density in Equation (8) is calculated as:

$$\rho = (1 - \alpha)\rho_1 + \alpha\rho_2. \tag{14}$$

The liquid- and gas-phase sonic velocities needed in Equation (8) are calculated with the relation derived from Equation (5):

$$c = \left(\frac{\partial p}{\partial \rho}\right)_s^{1/2} = \left(\frac{1}{\left(\frac{\partial \rho}{\partial p}\right)_h + \frac{1}{\rho}\left(\frac{\partial \rho}{\partial h}\right)_p}\right)^{1/2}. \tag{15}$$

The adopted value of the sonic velocity in oil is c_1 = 1000 m/s.

The derived critical flow model is validated for the conditions of water and air critical nozzle flow reported in [12]. The comparison between the calculated and the measured data is presented in Appendix A.

2.3. Subcritical Two-Phase Flow through Nozzles

The mass flow rate of refrigerant R744 and oil two-phase mixture through nozzles is calculated with the method presented in [15]. Pressure drop in two-phase flow through the nozzle is calculated as:

$$\Delta p = \Delta p_1 \phi_1^2 = \varsigma \frac{\rho_1 u_1^2}{2} \phi_1^2, \tag{16}$$

where ϕ_1^2 is the two-phase multiplier, ς stands for the flow resistance coefficient, and u_1 is the superficial liquid velocity (velocity in case that liquid-phase flows alone through the flow channel) upstream of the nozzle:

$$\dot{m}_1 = \rho_1 u_1 A, \tag{17}$$

where A is the area of the total cross-section of the flow channel. The two-phase mass flow rate through the nozzle is calculated as:

$$\dot{m} = \frac{\dot{m}_1}{(1 - \chi)}. \tag{18}$$

From Equations (16)–(18), it follows that

$$\dot{m} = \frac{A}{1-\chi}\left(\frac{2\Delta p \rho_1}{\varsigma \phi_1^2}\right)^{1/2}. \tag{19}$$

The two-phase multiplier is calculated as:

$$\phi_1^2 = 1 + CY + Y^2, \tag{20}$$

where Y corresponds to the reciprocal of the Lockhart–Martinelli parameter and according to [15] it is calculated as:

$$Y = \frac{C_1}{C_2}\frac{\chi}{1-\chi}\left(\frac{\rho_1}{\rho_2}\right)^{0.5} F. \tag{21}$$

In the above relations, the following notation applies. The ratio of the liquid- and gas-phase contraction coefficients is calculated as:

$$\frac{C_1}{C_2} = 0.666 \cdot 0.666^{-r}, \tag{22}$$

where r is the ratio of nozzle downstream and upstream pressure ($r < 1$). The correlation given by Equation (22) is obtained by the exponential regression of data from Table 13.1 in [15]. The constant C in Equation (20) is calculated as:

$$C = Z + \frac{1}{Z^2}, \tag{23}$$

$$Z = \frac{1}{S}\left(\frac{\rho_1}{\rho_2}\right)^{1/2}\frac{1}{Fr^{1/\kappa}}, \tag{24}$$

$$F = \left(\frac{1-r}{r^{2/\kappa}}\frac{1}{1-r^{(\kappa-1)/\kappa}}\frac{\kappa-1}{\kappa}\right)^{1/2}. \tag{25}$$

Velocity slip S in Equation (24) is calculated with Equations (11)–(13).

The flow resistance coefficient ζ in Equations (16) and (19) is evaluated for the liquid-phase flow through the nozzle according to the experimental correlation from [16]:

$$\begin{aligned}\varsigma = &\left[18.78 - 7.768 A_o/A_u + 6.337(A_o/A_u)^2\right]\cdot \\ &\exp\left\{\left[-0.942 - 7.246 A_o/A_u - 3.878(A_o/A_u)^2\right]\log \mathrm{Re}\right\}(A_u/A_o)^2\end{aligned} \tag{26}$$

where A_o denotes area of flow cross-section at the nozzle and A_u is the area of the upstream flow cross-section. The Reynolds number is evaluated for the nozzle velocity ($u_{1,0}$) and the hydraulic diameter:

$$\mathrm{Re} = \frac{u_{1,o} D_{h,o}}{\nu_1}. \tag{27}$$

The nozzle hydraulic diameter is $D_{h,o} = \frac{4A_o}{P_o}$ (where P_o is the perimeter of the nozzle flow cross-section) and ν_1 is the kinematic viscosity.

2.4. Refrigerant R744 (CO_2) Equation of State

The Peng–Robinson equation of state is adopted for the gas phase of CO_2 [17]:

$$p = \frac{RT}{V_m - b} - \frac{a\alpha}{V_m^2 + 2bV_m - b^2}, \text{ where} \tag{28}$$

$$a = \frac{0.457235 R^2 T_{cr}^2}{p_{cr}}, \tag{29}$$

$$b = \frac{0.077796RT_{cr}}{p_{cr}}, \tag{30}$$

$$\alpha = \left(1 + k\left(1 - T_r^{0.5}\right)\right)^2, \tag{31}$$

$$k = 0.37464 + 1.54226\psi - 0.26992\psi^2, \tag{32}$$

and $V_m = M/\rho$, $T_r = T/T_{cr}$, $M = 0.044$ kg/mol, $\psi = 0.228$, $R = 8.31446$ J/(molK), $T_{cr} = 304.25$ K, $p_{cr} = 73.9 \cdot 10^5$ Pa.

2.5. Solubility of CO_2 and PAG Oil

Figure 3 shows experimentally measured solubility of CO_2 in PAG oil [18]. According to [19], the CO_2 mass fraction in the mixture with oil is determined from:

$$\omega = (3.32p + 29.5)\exp\left(-1.6 \cdot 10^{-2}T\right)/100, \tag{33}$$

where pressure p is expressed in MPa and temperature T in °C. Comparison of the calculated and measured CO_2 mass fraction in the mixture with oil is presented in Figure 3. The good agreement is obtained for the higher mixture temperatures of 373.15 K, while up to 7% deviation is obtained for the lower temperature of 313.15 K. The results presented in the next Section 3 show that the influence of the CO_2 solubility on the mass flow rate and the back pressure predictions is small; therefore, some moderate deviations of the calculated values from the measured ones in Figure 3 do not have practical influence on the predicted mass flow rate and back pressure values. Based on the calculated ω values, the following parameters are predicted. The density of the liquid mixture of CO_2 and oil is calculated as:

$$\rho_1 = \frac{1}{\frac{\omega}{\rho_{CO_2}} + \frac{1-\omega}{\rho_o}}, \tag{34}$$

where subscript o denotes oil. The oil density is calculated as:

$$\rho_o = 1000 - 0.0008(T_o - 288), \tag{35}$$

where T is expressed in K.

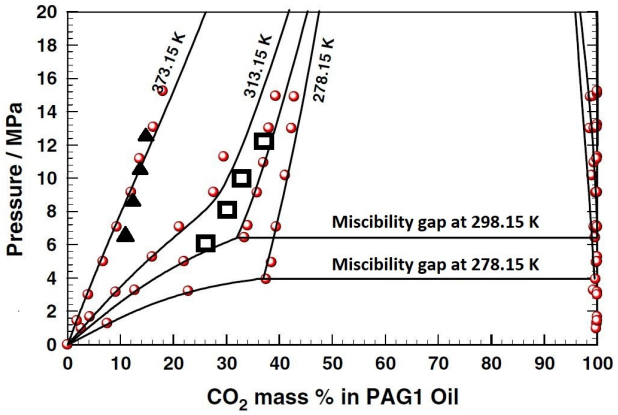

Figure 3. Solubility of CO_2 in PAG oil [18] (▲ and □ predicted with Equation (33), respectively, for 373.15 K and 313.15 K).

For defined oil mass fraction in the mixture with refrigerant:

$$g_0 = \frac{\dot{m}_o}{\dot{m}_o + \dot{m}_R} = \frac{\dot{m}_o}{\dot{m}_o + \dot{m}_2 + \omega\dot{m}_1}, \tag{36}$$

where index R denotes refrigerant, while subscripts 1 and 2, respectively, denote the liquid and gas phases. The mass flow rate fraction of the liquid phase is determined as:

$$1 - \chi = \frac{\dot{m}_o + \omega \dot{m}_1}{\dot{m}_o + \dot{m}_R} = g_o + \omega(1 - \chi), \tag{37}$$

which leads to the following expression for the flow quality:

$$\chi = 1 - \frac{g_o}{1 - \omega}. \tag{38}$$

Since CO_2 solubility in oil depends on pressure and temperature, values of CO_2 mass fraction in the mixture with oil in front of the high-pressure nozzle and in the back pressure chamber are not equal. The relation between these two values is derived from the balance of CO_2 mass flow rate:

$$\dot{m}_{2,BP} + \omega_{BP} \dot{m}_{1,BP} = \dot{m}_{2,in} + \omega_{in} \dot{m}_{1,in}, \tag{39}$$

where index in denotes flow parameters in front of the high-pressure nozzle and index BP parameters in the back pressure chamber. By dividing both sides of Equation (39) by the total fluid mass flow rate and by rearranging the equation, the flow quality in the back pressure chamber is obtained:

$$\chi_{BP} = \frac{\chi_{in}(1 - \omega_{in}) + \omega_{in} - \omega_{BP}}{1 - \omega_{BP}}. \tag{40}$$

In the performed calculation procedure, the flow quality in front of the high-pressure nozzle χ_{in} needed in Equation (40) is determined for specified g_o and ω, which is calculated for the defined pressure and temperature in the oil separator. The flow quality from the back pressure chamber towards the low-pressure nozzle is calculated using Equation (40).

3. Results

The two-phase flows of the refrigerant R744 and PAG oils through the high- and low-pressure nozzles in the connection from the oil separator at the compressor discharge side to the suction side, via the back pressure chamber, are calculated for the flow geometry presented in Section 2.1, applying the models presented in Sections 2.2–2.5. Calculations are performed for 10%, 50%, and 80% of the oil mass fraction in the mixture with refrigerant in the oil separator.

Four different pairs of pressure and temperature in the oil separator are considered: A(12 MPa,433 K), B(10 MPa,413 K), C(8 MPa,378 K), and D(6 MPa,353 K). These correspond to the ranges in the compressor typical discharge parameters. It is assumed that the temperature of the fluid in the back pressure chamber is equal to the arithmetic mean of the compressor suction and discharge temperatures. The suction pressure is 3.5 MPa and the corresponding suction temperature is 273 K. The back pressure value is determined iteratively by equating the mass flow rates through the high-pressure and low-pressure nozzles. The mass flow rate through the nozzle is calculated both by the critical flow model presented in Section 2.2 and by the subcritical flow model presented in Section 2.3. The lower value is adopted for the nozzle mass flow rate.

Figures 4–6 show refrigerant oil mass flow rates versus back pressure values, respectively, for cases with 80%, 50%, and 10% oil mass fractions in the oil separator. These predictions are performed by taking into account CO_2 solubility in oil with Equation (33). The mass flow rates from the compressor oil separator on the discharge side to the back pressure chamber are presented with black lines that show the constant values. These constant values indicate that the critical flow rate holds; this is because the flow rate depends on the upstream pressure, which is constant, but do not depend on the downstream pressure, which is variable. In case of the critical nozzle flow from the back pressure chamber to the

compression suction side, the mass flow rate increases moderately with the back pressure increase, as shown by the grey lines through points A and B in Figure 4, as well as through points A, B, and C in Figures 5 and 6. In the case of the subcritical nozzle flow from the back pressure chamber to the compression suction side, the mass flow rate rapidly increases with the back pressure increase, as shown by grey steep lines through points C and D in Figure 4, as well as through point D in Figures 5 and 6. As shown, the pressure in the back pressure chamber and the corresponding mass flow rate from the oil separator to the suction side via the back pressure chamber is determined through the cross-section of the line that presents the flow rate from the oil separator to the back pressure chamber and the line that presents the flow rate from the back pressure chamber to the compression suction side. The mass flow rate decreases with the decrease in the oil mass fraction, while the back pressure increases, as can be seen by comparing the values in the same points A, B, or C in Figures 4–6 (for instance, in case of 12 MPa and 160 °C in the oil separator, point A, the mass flow rates are 3.69×10^{-3} kg/s, 2.51×10^{-3} kg/s, and 1.71×10^{-3} kg/s, respectively, for 80%, 50%, and 10% of oil mass fraction in the oil separator at the discharge of the compressor; meanwhile, the values of the back pressure increase with the oil mass fraction decrease are, respectively, 4.76 MPa, 5.52 MPa, and 5.73 MPa). In cases with the oil separator under 6 MPa and 353 K (point D in Figures 4–6), the refrigerant and oil mixture flow from the back pressure chamber to the compressor suction side is subcritical and the back pressure is close to the suction pressure: the back pressure is very close to 3.5 MPa in cases with the oil mass fraction is 80% in the oil separator (Figure 4); meanwhile, in cases with 50% and 10% oil mass fractions in the oil separator, the back pressure is 3.65 MPa and 3.63 MPa, respectively (Figures 5 and 6).

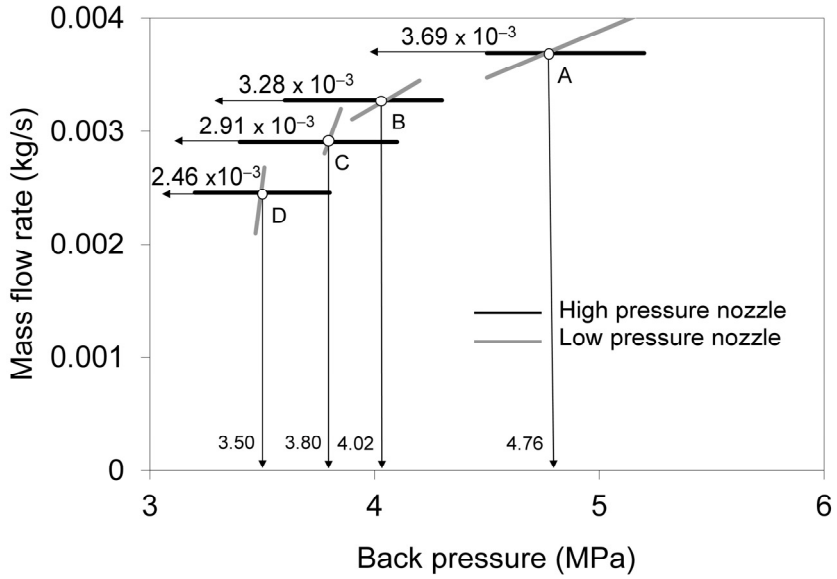

Figure 4. Back pressure values and mass flow rates through high-pressure and low-pressure nozzles for oil mass fraction in the oil separator of 80%. Prediction is performed by taking into account CO_2 and oil solubility. Pressure and temperature in the oil separator and temperature in the back pressure chamber are, respectively: A(12 MPa, 433 K, 353 K), B(10 MPa, 413 K, 343 K), C(8 MPa, 378 K, 325.7 K), and D(6 MPa, 353 K, 313 K).

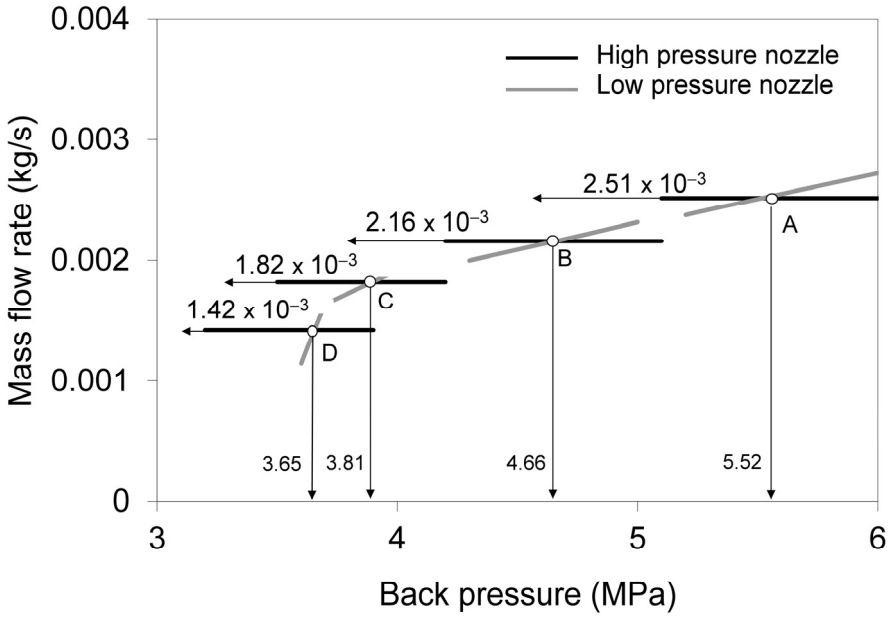

Figure 5. Back pressure values and mass flow rates through high-pressure and low-pressure nozzles for oil mass fraction in the oil separator of 50%. Prediction is performed by taking into account CO_2 and oil solubility. Pressure and temperature in the oil separator and temperature in the back pressure chamber are, respectively: A(12 MPa, 433 K, 353 K), B(10 MPa, 413 K, 343 K), C(8 MPa, 378 K, 325.7 K), and D(6 MPa, 353 K, 313 K).

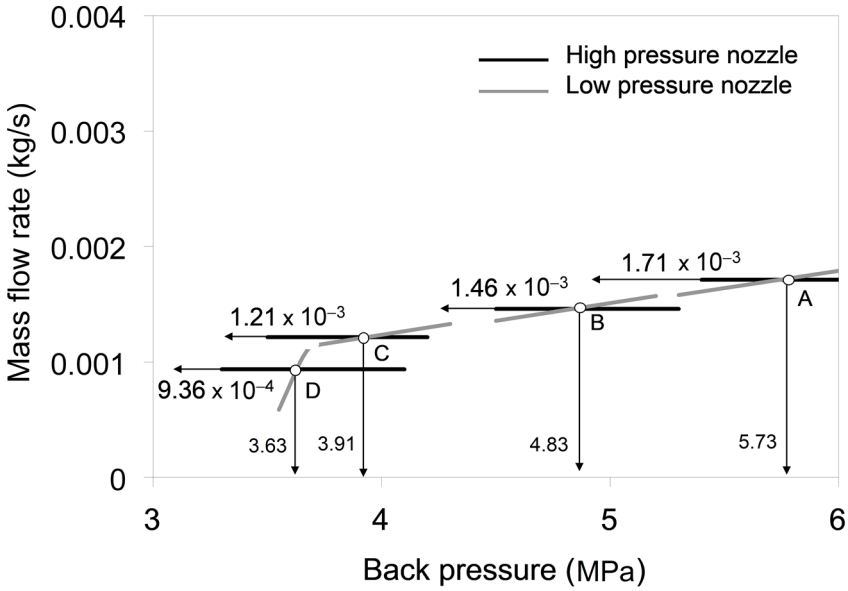

Figure 6. Back pressure values and mass flow rates through high-pressure and low-pressure nozzles for oil mass fraction in the oil separator of 10%. Prediction is performed by taking into account CO_2 and oil solubility. Pressure and temperature in the oil separator and temperature in the back pressure chamber are, respectively: A(12 MPa, 433 K, 353 K), B(10 MPa, 413 K, 343 K), C(8 MPa, 378 K, 325.7 K), and D(6 MPa, 353 K, 313 K).

Figures 7–9 show back pressure values and mass flow rates from the oil separator to the compressor suction side via the back pressure chamber for cases with 80%, 50%, and 10% of oil mass fraction in the oil separator, which are predicted under the assumption that there is no solubility of CO_2 in oil. By comparison of the cases calculated with and without the refrigerant dissolvement in oil under 80% oil mass fraction in the oil separator, Figures 4 and 7, it is shown that refrigerant dissolvement leads to the increase in

the refrigerant oil mass flow rate, which is more pronounced at the lower pressures. The corresponding values are: 2.46 over 2.14 g/s in case with 6 MPa in the oil separator (15% of mass flow increase due to the refrigerant dissolvement), 2.91 over 2.67 g/s in case with 8 MPa in the oil separator (9% of mass flow increase due to the refrigerant dissolvement), 3.28 over 3.16 g/s in case with 10 MPa in the oil separator (4% of mass flow increase due to the refrigerant dissolvement), and 3.69 over 3.63 g/s in case with 12 MPa in the oil separator (2% of mass flow increase due to the refrigerant dissolvement). The results of the back pressure in Figures 4 and 7 show that the refrigerant dissolvement leads to the notable decrease in pressure in the back pressure chamber under high pressures of 12 MPa and 10 MPa in the oil separator, while this difference is smaller under lower pressures of 8 MPa and 6 MPa in the oil separator. The differences of the predicted mass flow rates and back pressures in cases with and without refrigerant dissolvement under 50% and 10% oil mass fraction are smaller than in case with 80% of oil mass fraction in the oil separator. The comparison of results in Figures 5 and 8 for 50% oil mass fraction and Figures 6 and 9 for 10% of oil mass fraction show that the differences in the mass flow rates are practically negligible, while the differences in the back pressure are in the range within 0.18 MPa.

The back pressure decreases as the oil separator pressure decreases. For oil separator pressure values below 10 MPa, the back pressure is only a few fractions of MPa higher than the suction pressure of 3.5 MPa. In the case of the 80% oil mass fraction in the oil separator, the back pressure is 3.6 MPa for the oil separator pressure 6 MPa and it is 3.66 MPa for the oil separator pressure 8 MPa (Figure 5). In the case of the 10% oil mass fraction in the oil separator, the back pressure is 3.58 MPa and 3.87 MPa for the oil separator pressure 6 MPa and 8 MPa, respectively (Figure 7). Also, it is observed that the back pressure increases with the oil fraction decrease in the oil separator for oil separator pressures equal to or higher than 10 MPa. In the case of the 80% oil mass fraction in the oil separator, the back pressure is 4.3 MPa and 5.16 MPa for oil separator pressure that is equal to 10 MPa and 12 MPa, respectively (Figure 5); meanwhile, the back pressure rises to 4.77 MPa and 5.73 MPa in the case of 10% oil mass fraction in the oil separator (Figure 7).

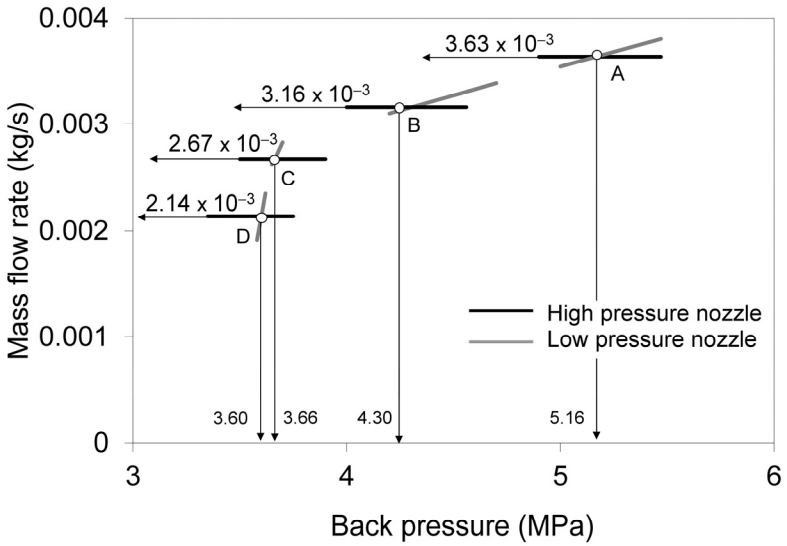

Figure 7. Back pressure values and mass flow rates through high-pressure and low-pressure nozzles for oil mass fraction in the oil separator of 80%. Prediction is performed under the assumption that CO_2 does not dissolve in oil. Pressure and temperature in the oil separator and temperature in the back pressure chamber are, respectively: A(12 MPa, 433 K, 353 K), B(10 MPa, 413 K, 343 K), C(8 MPa, 378 K, 325.7 K), and D(6 MPa, 353 K, 313 K).

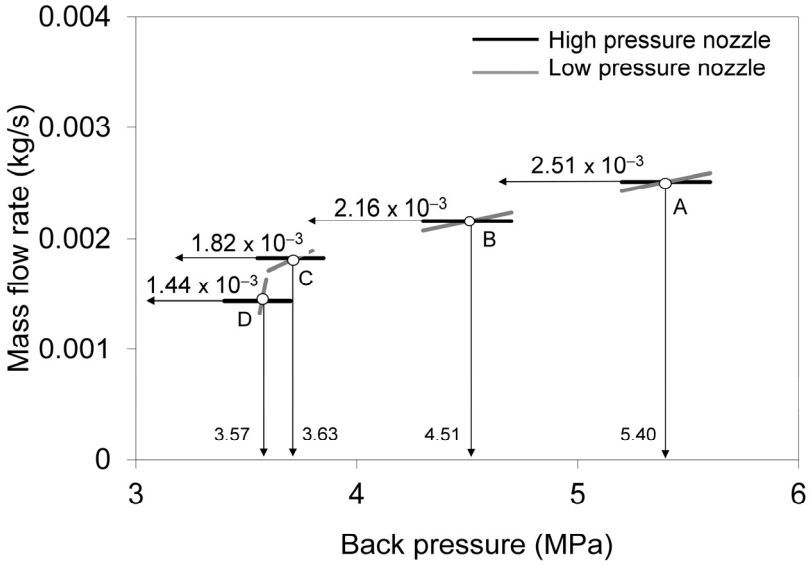

Figure 8. Back pressure values and mass flow rates through high-pressure and low-pressure nozzles for oil mass fraction in the oil separator of 50%. Prediction is performed under the assumption that CO_2 does not dissolve in oil. Pressure and temperature in the oil separator and temperature in the back pressure chamber are, respectively: A(12 MPa, 433 K, 353 K), B(10 MPa, 413 K, 343 K), C(8 MPa, 378 K, 325.7 K), and D(6 MPa, 353 K, 313 K).

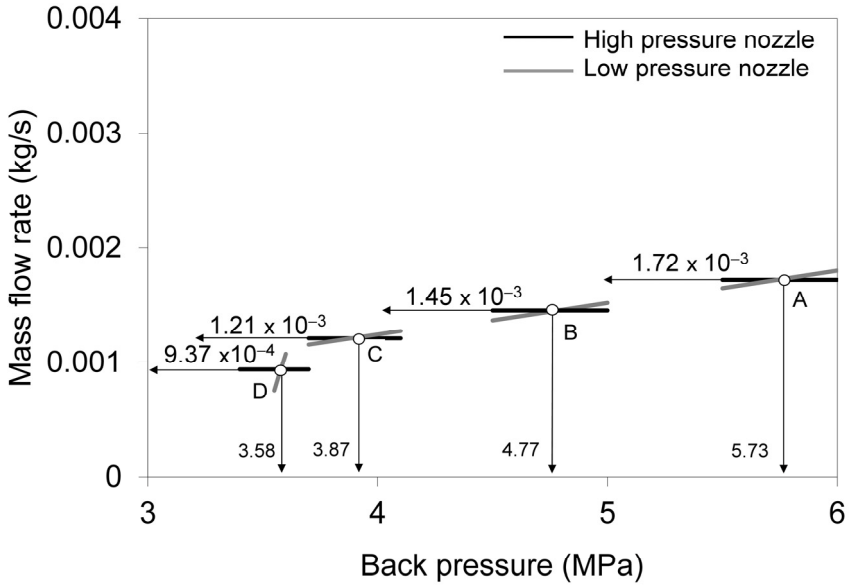

Figure 9. Back pressure values and mass flow rates through high-pressure and low-pressure nozzles for oil mass fraction in the oil separator of 10%. Prediction is performed under the assumption that CO_2 does not dissolve in oil. Pressure and temperature in the oil separator and temperature in the back pressure chamber are, respectively: A(12 MPa, 433 K, 353 K), B(10 MPa, 413 K, 343 K), C(8 MPa, 378 K, 325.7 K), and D(6 MPa, 353 K, 313 K).

4. Conclusions

The original models are developed for the prediction of the refrigerant oil critical and subcritical two-phase flows through the nozzle. The models take into account the slip between the liquid and gas phases and the refrigerant's solubility in oil. The model is validated for the experimental conditions of air–water critical flow through the small-diameter nozzle, which is the two-component gas–liquid two-phase flow condition equivalent to the refrigerant CO_2 gas and oil flow investigated in the present paper. The calculation of the

refrigerant CO_2 and PAG oil two-phase flow from the scroll compressor oil separator on the discharge side to the compressor suction side via the back pressure chamber is performed for a typical range of compressor operating parameters, with and without the refrigerant dissolvement in oil. The considered compression suction pressures and temperatures are 3.5 MPa and 273 K, while the discharge pressure and temperature are in the range from 6 MPa, 353 K to 12 MPa, and 433 K. The oil mass fraction in the oil separator was found to vary between 10% and 80%.

The major findings are as follows:

- The refrigerant oil two-phase flow from the oil separator to the back pressure chamber is critical. The refrigerant oil two-phase flow from the back pressure chamber to the compressor suction side is generally critical, but it becomes subcritical for lower discharge pressures and greater oil mass fractions. In all cases with the discharge pressure equal to 6 MPa, the flow through the nozzle between the back pressure chamber and the suction side is subcritical, while the increase in the oil mass fraction in the oil separator to 80% leads also to a subcritical flow in cases with an 8 MPa pressure in the oil separator.
- The increase in the oil mass fraction in the oil separator was found to lead to an increase in the mass flow rate from the oil separator to the compressor suction side, but to a decrease in the pressure value in the back pressure chamber. The oil mass fraction increase from 10% to 80% increases the mass flow rate by more than two times.
- The refrigerant dissolvement in oil contributes to a slight increase in the refrigerant oil two-phase mass flow rate and to a decrease in the back pressure. This mass flow rate change by refrigerant dissolvement in oil is more pronounced for greater oil mass fractions and lower compressor discharge pressures. For instance, the greatest increase in the mass flow rate by 15% is obtained for 80% oil mass fraction and 6 MPa in the oil separator. The back pressure change by refrigerant dissolvement in oil is more pronounced for greater oil mass fractions and higher discharge pressures. For instance, the greatest back pressure decrease—8%—was obtained for an 80% oil mass fraction and 12 MPa in the oil separator. In case of low oil mass fraction, the refrigerant dissolvement in oil has a negligible influence on flow parameters.

The modelling approach presented in this paper is original mechanistic approach. The developed critical flow model is based on the first principles through the application of the mass and energy balance equations (Equations (1) and (2)) of compressible isentropic flow (Equation (3)) of refrigerant CO_2 gas and PAG oil homogeneous mixture. The slip between the refrigerant gas phase and the oil liquid phase is taken into account through the Chislom and Zivi semi-empirical correlations (Equations (11)–(13)). The developed subcritical flow model is based on the well-established approach for the prediction of the two-phase flow pressure drop (Equation (16)), with the application of the two-phase multiplier (Equation (20)) and the experimental correlation for the prediction of the nozzle local flow resistance (Equation (26)); this is appropriate for flow conditions through small openings. Such an approach provides an engineering tool that is reliable and robust for the prediction of refrigerant gas and oil mixture flow through small openings, which is useful in the design of the scroll compressor with the back pressure sealing. As presented in Section 3, the pressure in the back pressure chamber is determined through the matching of the mass flow rates through the high-pressure and low-pressure nozzles.

Although the develop modelling approach is verified for the conditions of the critical air–water flow through small openings, the validation should be continued by comparison with the results of the future experiments that should be performed with the critical and subcritical flows of the refrigerant CO_2 and PAG oil mixtures. In addition, the application of the modelling approach to other type of refrigerants and lubricating oils requires introduction of appropriate equations of state, correlations for the prediction of corresponding thermophysical fluid parameters, and, if needed, the correlation for the prediction of refrigerant solubility in oil.

Author Contributions: Conceptualization, V.D.S.; Methodology, V.D.S.; Software, V.D.S. and M.M.P.; Validation, V.D.S. and M.M.P.; Resources, S.C.; Data curation, S.C.; Writing—original draft preparation, V.D.S. and M.M.P.; Writing—review and editing, V.D.S., M.I., M.M.P. and S.M. All authors have read and agreed to the published version of the manuscript.

Funding: This research was supported by the Science Fund of the Republic of Serbia through the Serbian Science and Diaspora Collaboration Program, #GRANT No 6403214, Multiphase Flows in Automotive Refrigeration Systems—MFARS.

Data Availability Statement: Data are contained within the article.

Conflicts of Interest: Stojan Cucuz was employed by the company Pierburg GmbH. The remaining authors declare that the research was conducted in the absence of any commercial or financial relationships that could be construed as a potential conflict of interest.

Nomenclature

A	area of flow cross-section, [m^2]
C	concentration coefficient, [-]
	constant in Equation (23), [-]
c	sonic velocity, [m/s]
c_p	specific isobaric heat capacity, [J/(kgK)]
D_h	hydraulic diameter, [m]
F	constant in in Equations (21), (24) and (25), [-]
g	mass fraction in the mixture with refrigerant, [-]
h	specific enthalpy, [J/kg]
M	molar mass, [kg/mol]
$\dot{m}$	mass flow rate, [kg/s]
P	perimeter, [m]
p	pressure, [Pa]
r	ratio of nozzle downstream and upstream pressure, [-]
R	universal gas constant, [J/(molK)]
R_g	gas constant, [J/(kgK)]
S	velocity slip, [-]
T	temperature, [K]
u	velocity, [m/s]
V_m	molar volume, [m^3/mol]
Y	the reciprocal of the Lockhart–Martinelli parameter, [-]
Z	constant in in Equations (23) and (24), [-]
Greek letters	
α	gas-phase volume fraction in two-phase mixture, [-]
ζ	local flow resistance coefficient, [-]
k	isentropic coefficient, [-]
n	kinematic viscosity, [m^2/s]
ρ	density, [kg/m^3]
ϕ_1^2	the two-phase multiplier, [-]
χ	flow quality, [-]
ψ	acentric factor, [-]
ω	refrigerant mass fraction in the mixture with oil, [-]
Indices	
1	liquid phase
2	gas phase
BP	in the back pressure chamber
c	the location of critical flow
cr	critical state
h	isenthalpic process
in	in front of the high-pressure nozzle
o	at the nozzle,
	Oil
p	isobaric process

R	refrigerant
s	isentropic process
u	the upstream location
Abbreviations	
PAG	polyalkylene glycol oil

Appendix A

The critical flow model presented in Section 2.2 is validated against measured data of air and water two-phase flow through the nozzle (measured data from the PUMA experimental facility [12]). The available air and water critical flow experimental conditions are chosen since they represent two-component, two-phase flows without phase change, which are the same conditions as those in the cases of oil and CO_2 flow. The inner diameter of the simulated test section tube was 24.4 mm, while the nozzle diameter was 5.4 mm. The obtained results [20] are presented in Figure A1 together with the predictions of the well-known Fauske model [21,22]. It is shown that Fauske model overpredicts the measured critical mass fluxes, while the present model shows an acceptable agreement with the measured data. Note that the values of the static quality x are depicted on the abscissa axis.

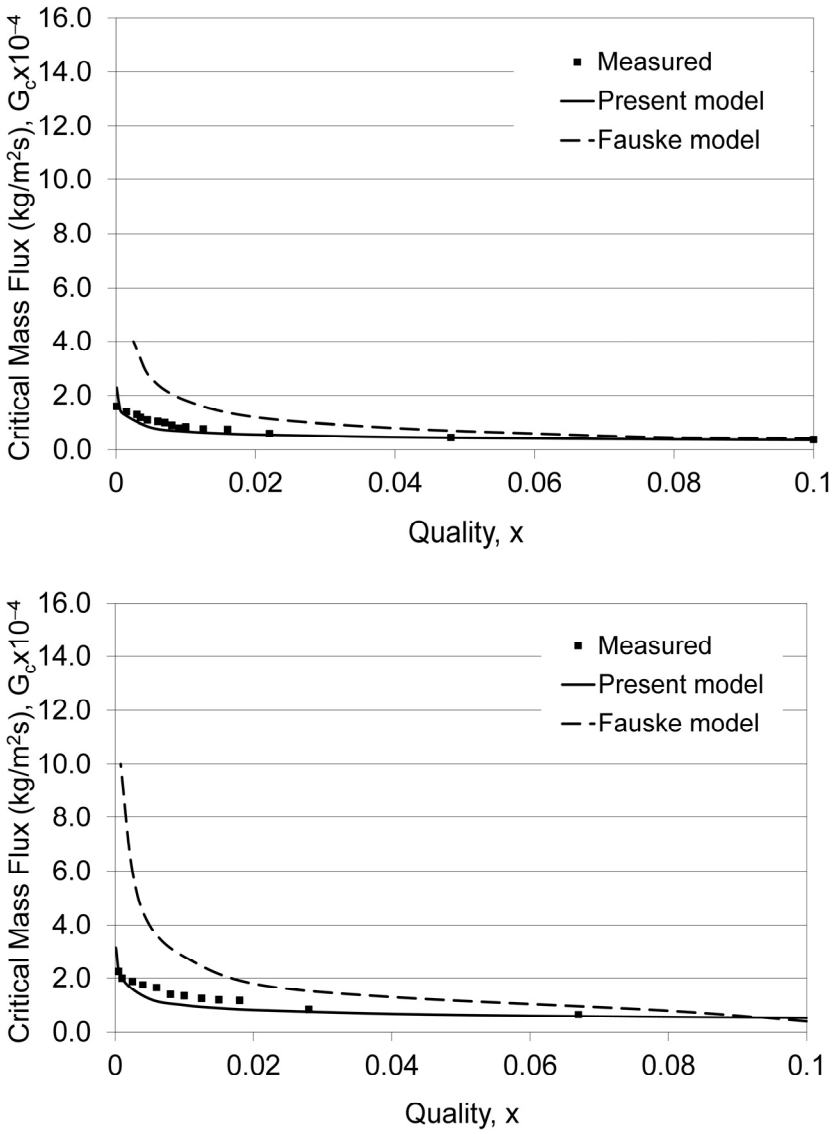

Figure A1. *Cont.*

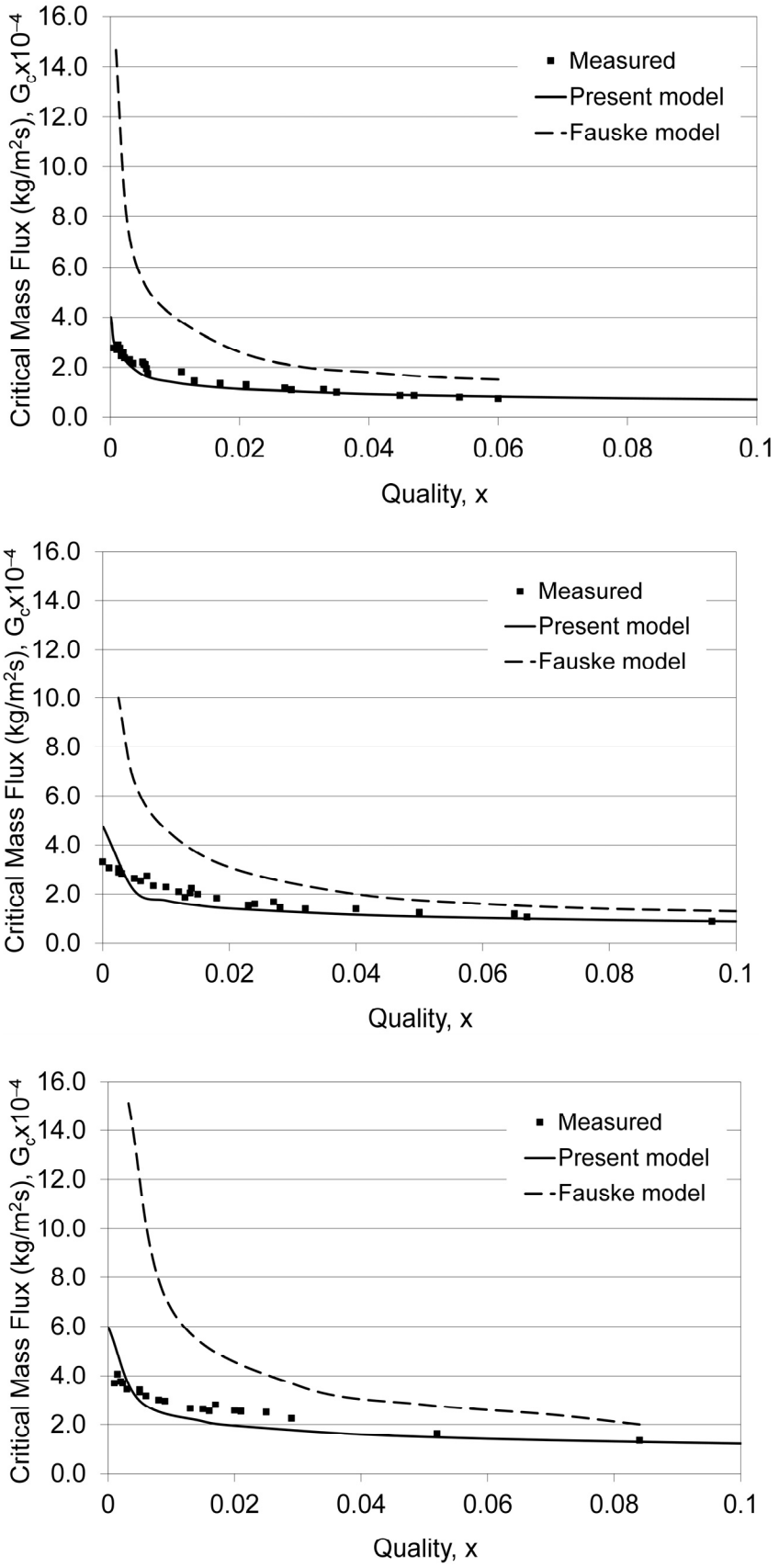

Figure A1. Comparison of measured and calculated choking mass fluxes. Experimental upstream pressure is from the top to the bottom diagram, respectively, 0.207 MPa, 0.345 MPa, 0.517 MPa, 0.689, 1.034 MPa.

References

1. Richardson, H.; Gatecliff, G. Comparison of the high side vs low side scroll compressor design. In Proceedings of the International Compressor Engineering at Purdue, West Lafayette, IN, USA, 14–17 July 1992. Available online: https://docs.lib.purdue.edu/icec/852 (accessed on 17 November 2023).
2. Tang, Y.; Hung, C.; Chang, Y. Performance improvements in low side scroll compressor with extended operation speeds. *Appl. Therm. Eng.* **2011**, *31*, 3542–3551. [CrossRef]
3. Qian, Z.; Zhang, Z. Back-pressure mechanism of scroll compressor. In Proceedings of the International Compressor Engineering Conference, West Lafayette, IN, USA, 14–17 July 1992. Available online: https://docs.lib.purdue.edu/icec/909 (accessed on 17 November 2023).
4. Ghiaasiaan, S.M. *Two-Phase Flow, Boiling and Condensation*; Cambridge University Press: Cambridge, UK, 2008.
5. Kim, Y.; O'Neal, D.L. The effect of oil on the two-phase critical flow of Refrigerant 134a through short tube orifices. *Int. J. Heat Mass Transf.* **1994**, *37*, 1377–1385.
6. Zhang, Z.; Tian, L.; Tong, L.; Chen, Y. Choked Flow Characteristics of Subcritical Refrigerant Flowing Through Converging-Diverging Nozzles. *Entropy* **2014**, *16*, 5810–5821. [CrossRef]
7. Kim, M.K.; Lee, H.; Jeong, J.H. Evaluation of correlations for mass flow rate of refrigerant through electronic expansion valve in air—Water heat pump system using R32. *Int. J. Refrig.* **2023**, *151*, 267–277. [CrossRef]
8. Nikolov, A.; Brümmer, A. Two-phase mass flow rate through restrictions in liquid-flooded twin-screw compressors or expanders. *Int. J. Refrig.* **2023**, *148*, 152–167. [CrossRef]
9. Tojo, K.; Hayase, I. Self-Adjusting Back Pressure Mechanism for Scroll Compressors. In Proceedings of the International Compressor Engineering Conference, West Lafayette, IN, USA, 23–26 July 1996. Available online: https://docs.lib.purdue.edu/icec/1356/ (accessed on 17 November 2023).
10. Tojo, K.; Hayase, I.; Tsuchiya, T. Improvement of Self-Adjusting Back Pressure Mechanism for Scroll Compressors. In Proceedings of the International Compressor Engineering Conference, West Lafayette, IN, USA, 14–17 July 1998. Available online: https://docs.lib.purdue.edu/icec/1499/ (accessed on 17 November 2023).
11. Beskok, A.; Karniadakis, G.; Trimmer, W. Rarefaction and Compressibility Effects in Gas Microflows. *J. Fluids Eng.* **1996**, *118*, 448–456. [CrossRef]
12. Yoon, H.J.; Ishii, M.; Revankar, S.T. Choking flow modelling with mechanical non-equilibrium for two-phase two-component flow. *Nucl. Eng. Des.* **2006**, *236*, 1886–1901. [CrossRef]
13. Grolmes, M.A.; Fauske, H.K. Comparison of the Propagation Characteristics of Compression and Rarefaction Pressure Pulses in Two-Phase, One-Component Bubble Flow. *Trans. Am. Nucl. Soc.* **1968**, *11*, 6833.
14. Whalley, P.B. *Two-Phase Flow and Heat Transfer*; Oxford University Press: Oxford, UK, 1996.
15. Chisholm, D. *Two-Phase Flow in Pipelines and Heat Exchangers*; George Godwin: London, UK, 1983; pp. 200–214.
16. Idelchik, I.E. *Handbook of Hydraulic Resistance*; Mashinostroenie: Moscow, Russia, 1992; p. 175. (In Russian)
17. Peng, D.Y.; Robinson, D.B. A new two-constant equation of state. *Ind. Eng. Chem. Fundam.* **1976**, *15*, 59–64. [CrossRef]
18. Yokozeki, A. Solubility correlation and phase behaviours of carbon dioxide and lubricant oil mixtures. *Appl. Energy* **2007**, *84*, 159–175. [CrossRef]
19. Dang, C.; Arai, S. Numerical simulation of two-phase flow pattern of supercritical carbon dioxide with PAG-type lubricating oil in gas cooler. In Proceedings of the International Refrigeration and Air Conditioning Conference, West Lafayette, IN, USA, 16–19 July 2012. Available online: http://docs.lib.purdue.edu/iracc/1339 (accessed on 17 November 2023).
20. Petrovic, M.M.; Stevanovic, V.D. Two-component two-phase critical flow. *FME Trans.* **2016**, *44*, 109–114. [CrossRef]
21. Fauske, H.K. *Contribution to the Theory of Two-Phase, One-Component Critical Flow*; Argonne National Laboratory Report ANL-6633; Argonne National Lab.: Lemont, IL, USA, 1962.
22. Henry, R.E.; Fauske, H.K. The two-phase critical flow of one composition mixtures in nozzle, orifices, and short tubes. *J. Heat Transf.* **1971**, *93*, 179–187. [CrossRef]